Towards time-resolved multi-property measurements by single-frequency FRS

Ulrich Doll[1,*], Ralf Kapulla[2], Michael Dues[3], Jonas Steinbock[3], Sergey Melnikov[3], Ingo Röhle[4], Matteo Migliorini[5], Pavlos K. Zachos[5]
1: Department of Mechanical and Production Engineering, Aarhus University, Denmark
2: Experimental Thermal Hydraulics Group, Paul Scherrer Institute (PSI), Switzerland
3: ILA R&D GmbH, Germany
4: Berliner Hochschule für Technik, Germany
5: Centre for Propulsion and Thermal Power Engineering, Cranfield University, United Kingdom
* Corresponding author: ud@mpe.au.dk

Keywords: filtered Rayleigh scattering, multi-property, simultaneous, time-resolved, pressure, temperature, flow velocity, multiple views

ABSTRACT

The filtered Rayleigh scattering technique (FRS), extended by the method of frequency scanning, has historically been limited to time-averaged multi-property flow measurements. In our recently published work, we present a concept that, based on the observation of the region of interest from six perspectives and a single excitation frequency, potentially enables the combined measurement of time-resolved pressure, temperature and three-component (3C) velocity fields. This work summarizes and expands on a follow-up publication that experimentally verifies this concept on an aspirated circular duct flow. This is accomplished by comparing the results obtained from single-frequency data processing to reference pressures and temperatures and corresponding LDA velocity measurements. An overall very good agreement with accuracies of 3.4% in pressure and 1.3% in temperature and ±2 m/s in axial velocity is found for all operating points. Concerning precision, a newly developed multistage evaluation procedure enables values for pressure, temperature and velocity as low as 3 hPa, 2.2 m/s and 1.7 m/s. In a second flow configuration, an axial swirler is introduced into the duct. The resulting secondary flow structure and deformation of the axial velocity field caused by swirler geometry and support are very well captured with the single-frequency analysis. A closing discussion on the implementation challenges of a single-frequency multi-property FRS instrument with pulsed laser radiation reveals significant obstacles to overcome. Due to a identified considerable optimization potential, chances are high that true time-resolved multi-property measurements by FRS will become a reality.

1. Introduction

The filtered Rayleigh scattering (FRS) technique (R. Miles & Lempert, 1990), extended by the frequency scanning method (Boguszko & Elliott, 2005; Doll et al., 2014; Forkey et al., 1996) has the demonstrated ability to measure pressure, temperature and 3-component (3C) velocity fields simultaneously (Doll et al., 2017). However, since frequency scanning is time consuming, the multi-property measurement abilities of FRS have so far been limited to time-averaged measurements. To harness the unique potential of FRS for the combined measurement of multiple time-resolved flow quantities, the measurements need to be based on pulsed laser light with only

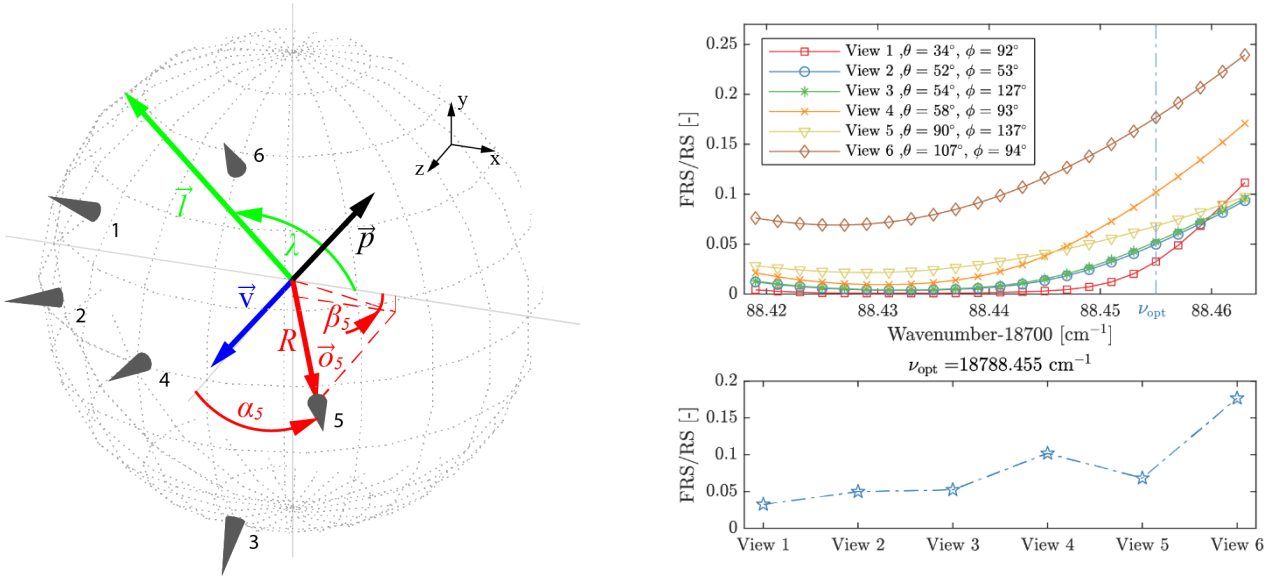

Figure 1: (left) Orientation of the six optimised camera views on a sphere around the region of interest. (Right, top) Simulated FRS intensity spectra normalised by the available Rayleigh scattering (RS) for a frequency scan around the 18788.44 cm-1-doublet for the six optimised camera views. The scattering angles $\boldsymbol{\phi}, \boldsymbol{\theta}$ are indicated in the legend. Bottom FRS signal intensities at the optimised single-pulse wavenumber $\boldsymbol{\nu_{opt}}$.(Doll et al., 2024).

a single excitation frequency. To this end, our recent article develops a diagnostic concept based on the use of multiple optimized perspective views (Doll et al., 2022). The resulting six-view detection concept is subsequently installed on an aspirated pipe flow experiment, where frequency scanning measurements based on continuous wave (CW) laser illumination are conducted (Doll et al., 2024). In addition, the data are analyzed based on a single excitation frequency to obtain quasi-time-resolved measurements of pressure, temperature and the three velocity components.

It is the intention of this paper to expand on this recently published work. After a brief introduction to the underlying principle of the multi-view FRS approach, the experimental setup and FRS instrumentation are introduced. This is followed by a presentation of experimental results for a straight and a swirled pipe flow configuration. Finally, the paper focuses on the future development lines to ultimately implement a time-resolved multi-property FRS instrument.

2. Multi-view FRS and instrumentation

The measurement of multiple flow properties by FRS can be perceived as an underdetermined mathematical problem, where an intensity value detected at a camera pixel stands against the five wanted flow variables, namely pressure, temperature and the three velocity components. Furthermore, the measurement of the three velocity components based on the optical Doppler frequency shift requires a variation either in laser or observer direction. By combining three camera views with frequency scanning, the additional intensity values obtained at each resoluion

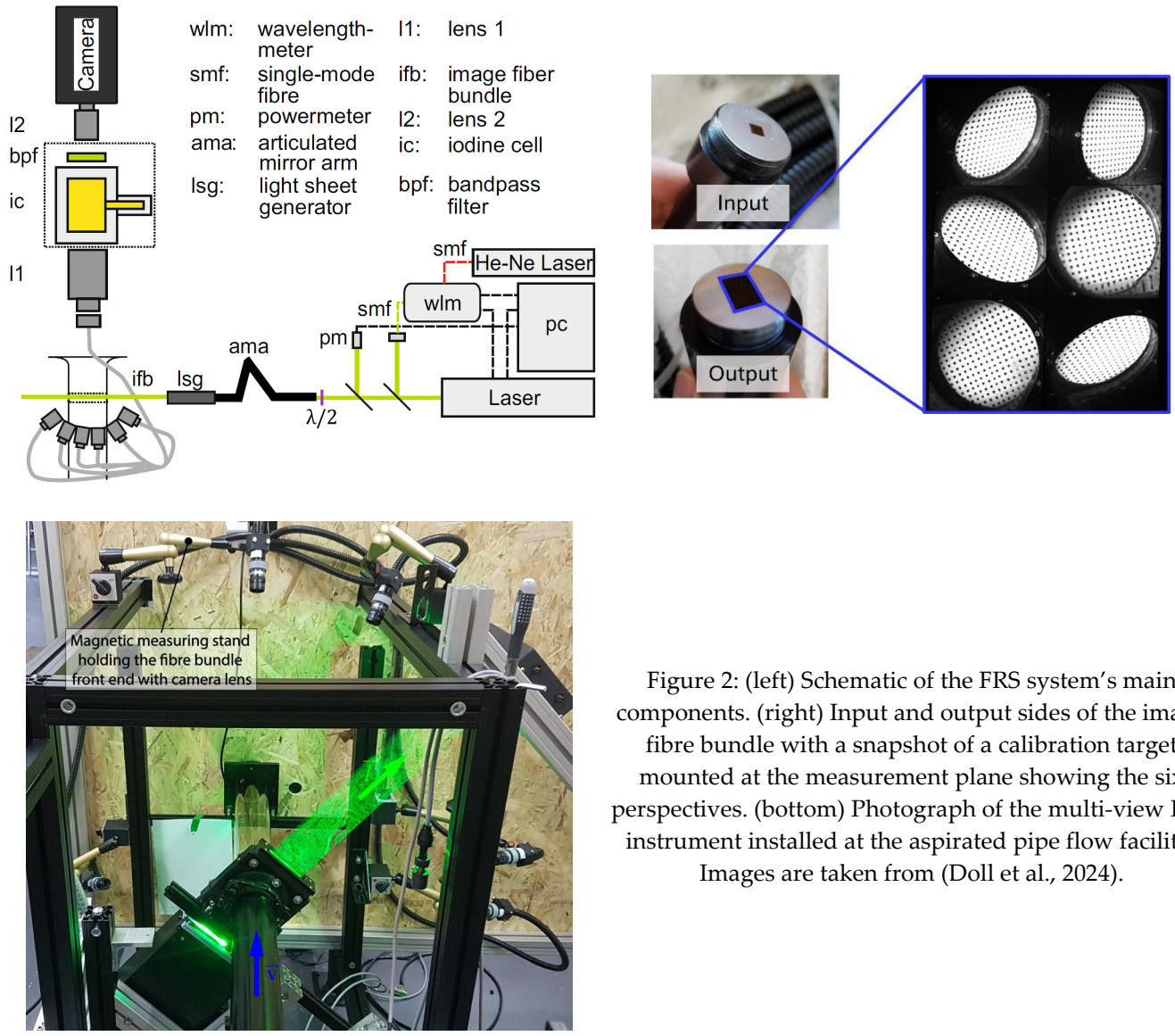

Figure 2: (left) Schematic of the FRS system's main components. (right) Input and output sides of the image fibre bundle with a snapshot of a calibration target mounted at the measurement plane showing the six perspectives. (bottom) Photograph of the multi-view FRS instrument installed at the aspirated pipe flow facility. Images are taken from (Doll et al., 2024).

element turn the evaluation task into an overdetermined system of equations and regression algorithms can be used to derive the flow quantities with high accuracy (Doll et al., 2017). However, this approach is limited to time-averaged measurements. The basic idea to enable the time-resolved measurements of the five flow variables is to increase the number of perspective views to an equal number of five or more so that a unique mathematical solution can be found (Doll et al., 2022).

Compared to the number of individual frequencies that can be realized in a frequency scan, the number of camera views which can be implemented is naturally limited. In order to reach the lowest possible measurement uncertainties in a single-fequency multi-view FRS setup, the placement of the different perspective views is vital and an optimization tool is introduced to determine an optical configuration with the highest achievable flow parameter sensitivities (Doll

et al., 2022). A schematic representation of the six-view observation concept implemented in this work is shown in Figure 1 (left). The camera perspectives are located on a spherical surface with the sphere radius determined by the object size (i.e. the illuminated cross section) and the collection optics so that their individual positions are determined by the polar and azimuthal angles α and β. The laser is oriented at an angle of 45° in the x-y plane to ensure uniformly distributed uncertainties for the in-plane velocity components. The resulting normalized intensities are a strong function of the scattering geometry for each camera perspective, Figure 1 (right, top). The angles θ and ϕ between laser and observation direction and polarization and observation direction represent this influence on the FRS signal; while θ has a distinct impact on the spectral shape of the Rayleigh scattering, ϕ accounts for its dipole nature (R. B. Miles et al., 2001). For a single-frequency measurement, the corresponding intensities are then selected at an optimized excitation frequency ν_{opt}, Figure 1 (right, bottom).

A schematic overview of the of the multi-view FRS instrument is presented in Figure 2 (left). The system utilizes a 532 nm continuous-wave (CW) Azur-Light fiber laser. This laser provides adjustable output power ranging from 0.1 to 6 W, operated at 5 W. A narrow spectral linewidth below 200 kHz is achieved by an external NKT Photonics ADJUSTIK Y10 seed laser unit. The laser incorporates both fast piezo and thermal tuning mechanisms, allowing precise adjustments to its output frequency. Piezo tuning covers a fine-grained 10 GHz range, while thermal tuning provides access to a broader 700 GHz emission spectrum. To actively control the laser frequency, a portion of laser light is sampled into a HighFinesse WS8 wavelength-meter (wlm) and a built-in controller is used to maintain a deviation of less than 1 MHz from the set value. To compensate for thermal variations, the device undergoes regular calibration using a frequency-stabilized Helium-Neon (He-Ne) laser. Additionally, a secondary branch continuously monitors the laser's output power using a power meter (pm). The primary laser beam is directed through an articulated mirror arm (ama) into a light sheet generator (lsg), which expands the beam to a height of approximately 100 mm using an optical scanner arrangement. A half-wave plate ($\lambda/2$) is used to align the polarization of the laser beam to the laser sheet plane.

Light collection from the measurement plane is based on a six-branch image fiber bundle (ifb) that facilitates the acquisition of six different perspective views using a single camera system (PCO Edge 4.2). Each branch is equipped with a camera lens (1.4 f-number, 16 mm focal length) that focuses the captured light onto the square fiber bundle input side, that consists of 400 x 400 fibers with 10 µm core diameter and a specified transmission of 40%. The six perspectives are combined at the distal end of the device, forming a rectangular light sensitive area of 12 x 8 mm^2. Photographs of the input and output sides of the image fiber bundle as well as an image of a

calibration plate are shown in Figure 2, right. All six views are combined merged in a single camera frame, where each of the square sections belongs to an individual camera perspective. Finally, the light collected from the measurement plane is conditioned by an iodine filter cell (ic) and a bandpass filter (bpf, FWHM 10 nm) inside the transfer optics (l1, l2) before reaching the camera sensor. For all measurements, the camera's exposure time is set to 20 s and a 4 x 4 binning is applied.

The multi-view FRS instrument is installed on an aspirated pipe flow facility as shown in Figure 2, bottom. Air is sucked in through a bell-shaped inlet nozzle and a flow conditioning section, and streams through a round pipe with 80 mm inner diameter. Further downstream, the light sheet illuminates the channel cross section through a tiny slit left between the inlet pipe and the transparent measuring section to avoid laser interference with the glass surfaces. The following precision borosilicate glass channel has a length of 500 mm with anti-reflective coating. According to optimized camera configuration in Figure 1, left, the six fiber bundle front ends are positioned downstream of the light sheet plane using flexible magnetic stands. For more information regarding the alignment procedure and associated uncertainties please refer to (Doll et al., 2024). The black flexible hoses contain fiber bundles and are combined at the rear end of the device behind the wooden screen.

3. Data processing and results

3.1 General procedure

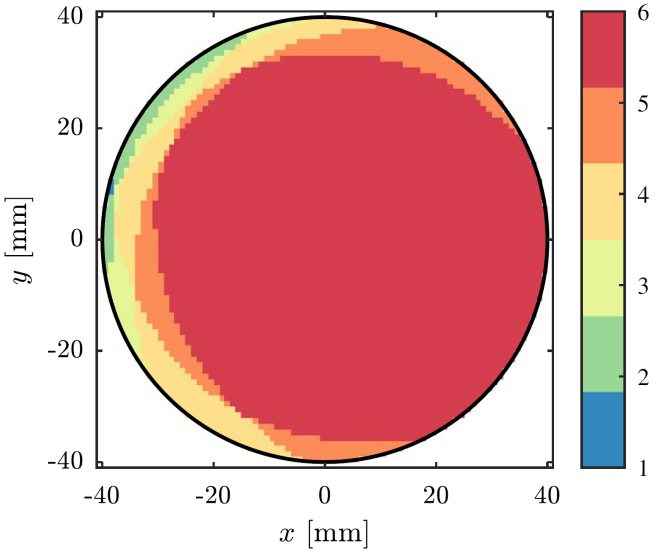

Figure 3: Spatial overlap of the camera perspectives (Doll et al., 2024).

This section only provides a brief summary of the data processing steps. For more detailed information the reader is kindly referred to our recent journal paper (Doll et al., 2024).

The FRS instrument acquires data in a multi-step process. First, a calibration phase involves capturing a set of calibration target images to determine camera positions and map different viewpoints onto a common grid. Then, reference measurements are acquired under controlled conditions of pressure, temperature, and zero flow velocity. This reference data is used to calculate an optical calibration constant, a background parameter, and a zero Doppler shift

to account for the accuracy of the wavelengthmeter and frequency-dependent properties of the bandpass filter. Finally, data is collected under actual flow conditions. Both the reference and flow data involve frequency scans at 37 discrete steps, with measurements repeated five times and averaged to improve signal-to-noise ratio. To fully evaluate the FRS data, information about the transmission curve of the absorption filter, previously calibrated with a photodiode arrangement to an accuracy of less than 0.5%, is required.

To account for spatial noise that is introduced by the fiber structure of the image fiber bundle, all FRS data images are smoothed with a 3 x 3-pixel spatial averaging filter before further processing. Calibration constant, background parameter and zero Doppler shift are determined for each pixel and perspective separately. These parameters are then further used in the analysis of the flow data, where the information of all six perspectives is combined to simultaneously determine pressure, temperature and the three velocity components.

Due to the facility's support structure, part of the flow channel is obstructed from view for certain perspectives. This is indicated in Figure 3, where the color code represents the number of usable perspectives per resolution element. For the frequency scanning analysis, three perspectives are sufficient to determine the five flow parameters so that almost the complete cross section is covered. With three to six perspectives and 37 scanning frequencies, this results in 111 to 222 measured intensities per resolution element, which results in a robust, significantly overdetermined mathematical problem. In contrast, the single frequency evaluation has to rely on only six intensities per resolution element, which makes the analysis more sensitive to bias errors or statistical uncertainty. To tackle this issue, a multi-stage data fitting method has been devised. This approach leverages an empirical observation indicating that velocity components can be accurately determined even in the absence of precise knowledge about the thermodynamic properties. Consequently, the multi-stage procedure commences by solely fitting the three velocity components, while maintaining pressure and temperature at their initial estimates. Subsequently, the obtained velocities are utilized in a secondary fitting process where the velocities remain constant, and adjustments are made to pressure and temperature. This iterative process continues until the resulting flow characteristics converge towards a specific value. In the present scenario, it was noted that the multi-stage fitting technique produces satisfactory outcomes after just one iteration, potentially due to the limited interaction between thermodynamics and aerodynamics in the current flow experiment. The same Levenberg-Marquardt fitting algorithm is used for both frequency scanning and single frequency evaluation.

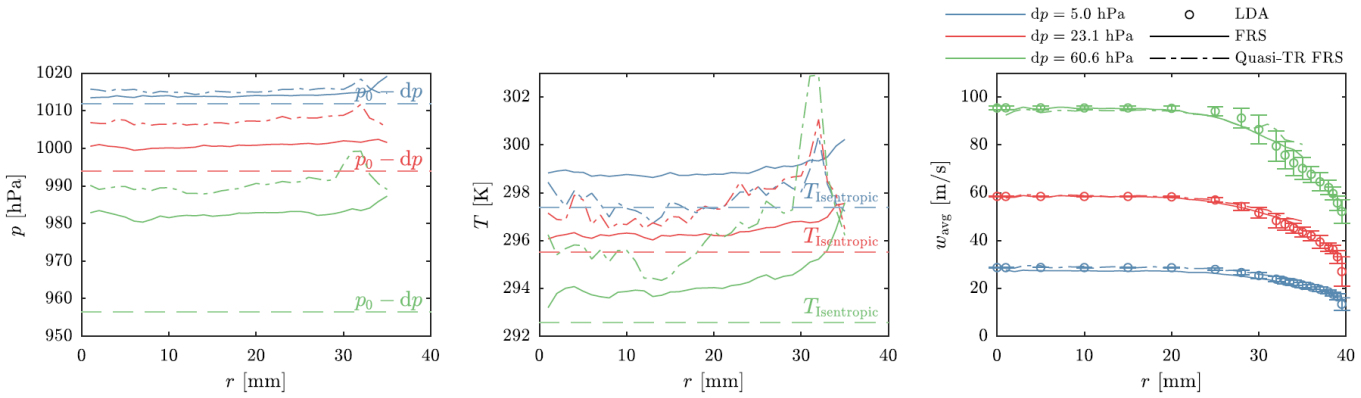

Figure 4: Comparison of radially averaged FRS results with pressure profiles with $\boldsymbol{p_0 - dp}$ (dashed) (a), with isentropic temperature calculations (dashed) (b) and LDA measurements (circles) (c) for frequency scanning (solid) and single-frequency data analysis (dashed-dotted). The three operating points denoted by the differential pressure $\boldsymbol{dp}$. LDA errorbars in (c) indicate the standard deviation of the radial mean velocity per radius (Doll et al., 2024).

3.2 Straight flow

The straight flow case is well suited to analyze the uncertainty bounds of the single-frequency approach, since the spatial plug flow structure consists of areas of constant flow parameters, so that the spatial variation of the FRS results can be interpreted as statistical uncertainty. The most important conclusions of (Doll et al., 2024) are summarized here and the reader is again kindly referred to the paper for a comprehensive analysis.

To evaluate the accuracy of the FRS measurements, radially averaged pressure, temperature, and axial velocity profiles obtained from frequency scanning and single-frequency (quasi-time-resolved) analyses are compared to reference values. This includes the differential pressure dp at the inlet nozzle, resulting isentropic temperature, and corresponding laser Doppler anemometry (LDA) velocity measurements for three distinct bulk velocities indicated as depicted in Figure 4. The average differences between FRS results and reference values for pressure profiles increase with the flow rate, ranging from 2 to 27 hPa (0.2 to 2.8%) for frequency scanning and 3 to 33 hPa (0.3 to 3.5%) for quasi-time-resolved analysis. Deviations in isentropic temperatures peak at approximately 3.8 K (1.3%) for the highest flow rate in the quasi-time-resolved analysis, while remaining below 2.1 K (0.7%) for other configurations. Comparison of axial velocities measured by LDA and FRS within a radial distance of r = 25 mm demonstrates strong agreement across all operational points and data processing methods, with discrepancies falling within ±2 m/s (7 to 2% of maximum velocity). The increasing deviations near the channel boundaries can be attributed to variations in measurement locations; LDA measurements were taken 2-3 tube diameters downstream, resulting in a more developed velocity profile with a smaller region of constant velocity near the center and gentler slopes towards the channel periphery.

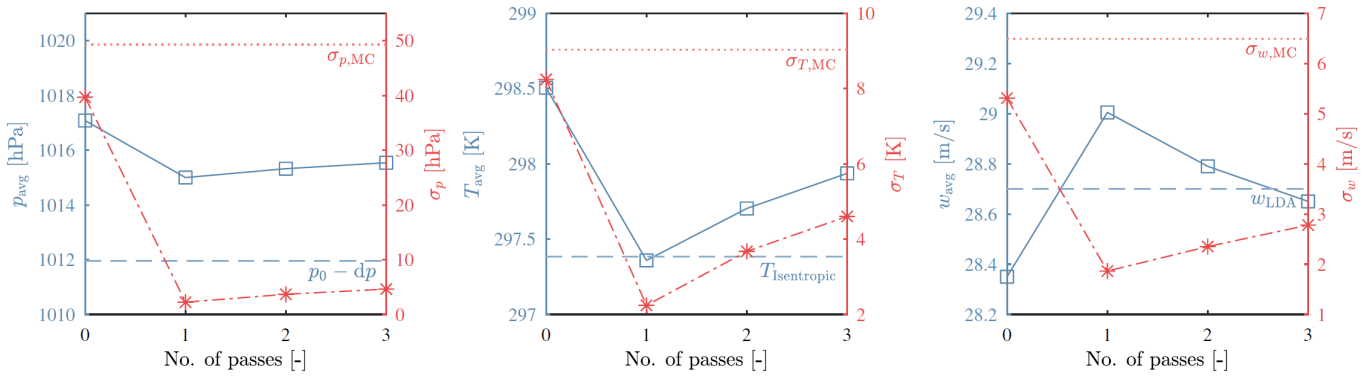

Figure 5: Spatial averages (blue, solid) and standard deviations $\boldsymbol{\sigma}$ (red, dashed-dotted) of the constant core flow region at operating point $\mathbf{dp}$ = 5.0 hPa plotted against the number of multistage passes (zero means conventional fitting) for $\boldsymbol{p}$ (left), $\boldsymbol{T}$ (middle) and $\boldsymbol{w}$ (right). Reference values are represented by the blue dashed lines. Standard deviations $\boldsymbol{\sigma_{MC}}$ (red, dotted) are theoretical values computed from Monte-Carlo simulations (Doll et al., 2024).

All quasi-time-resolved results presented in this study are achieved using the multistage evaluation method outlined above. An assessment of mean convergence and precision is conducted against the number of iterations through the multistage fitting process, as shown in Figure 5. Given the flow's constant properties in the core region, spatial standard deviations are indicative of measurement precision for each flow parameter. Spatial averages suggest convergence is feasible both when fitting all flow parameters simultaneously (zero iterations) and when varying the number of iterations of the multistage fitting, as observed changes fall within precision limits. Notably, transitioning from conventional to multistage evaluation results in a significant reduction in standard deviations from 40 to 2.2 hPa (4 to 0.2%) for pressure, 8.2 to 2.2 K (2.8 to 0.8%) for temperature, and 5.3 to 1.7 m/s (18.7 to 6.4%) for axial velocity after a single multistage iteration, followed by a gradual increase with additional passes. The cause of decreased precision after two or more iterations remains unknown and warrants further investigation. While conventional fitting aligns closely with theoretical values derived from Monte Carlo simulations, slight discrepancies may be attributed to initial spatial image smoothing. In summary, the single-pass multistage fitting approach significantly enhances precision by factors of approximately 3 and 4 for axial velocity and temperature, and by a factor of 18 for pressure.

3.3 Swirling flow at 7 D

To demonstrate the ability of the multi-property single frequency FRS approach to resolve secondary flow patterns, an axial swirler is designed (Figure 6) and introduced into the flow channel 7 diameters upstream of the measurement plane.

A comparison of velocity, pressure and temperature maps obtained with both processing methodologies are presented in Figure 7. The bulk flow velocity exhibits perturbations associated

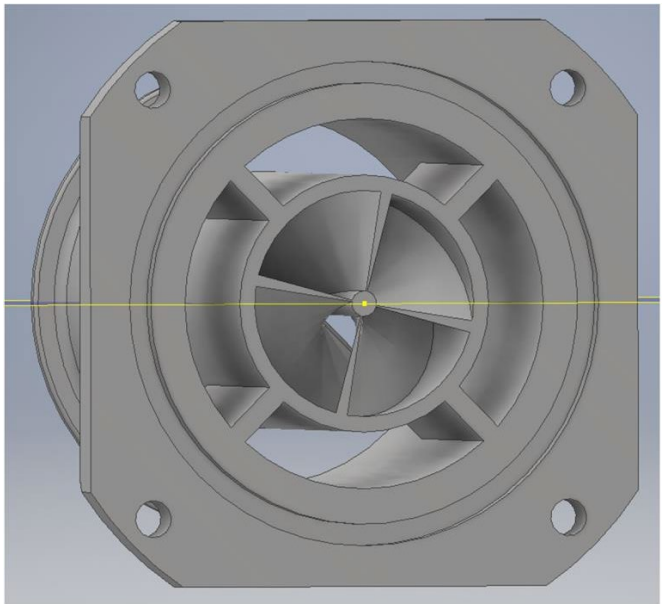

Figure 6: 3D rendering of the axial swirler.

with the wakes of the swirler blades and the axial swirler's support structure, leading to a notable velocity deficit in the center. The in-plane velocities are dominated by the flow's rotational motion. Both processing methods capture these features very well. While frequency scanning results are available for almost the entire cross section, the single-frequency data are confined to the overlap area of all six perspectives and contain more spatial noise. Pressure and temperature are expected to be constant over the channel cross section, which is well represented by the results of both methods. While the single-frequency results appear grainier but overall, very smooth, the frequency scanning results contain several spatial artifacts. The circle shaped structures are related to channel boundaries that are blocking the field of view for certain perspectives and are naturally not present in the single-frequency maps, as only the overlap area corresponding to all six views is used. Additionally, the frequency scanning pressure field shows a diagonal low-pressure stripe and somewhat higher pressure zones at the boundaries that are potentially caused by frequency dependencies of the calibration constant and the background parameter. As outlined in (Doll et al., 2024), these parameters are obtained for a significantly smaller frequency range around the optimized excitation frequency for the single-frequency analysis as compared to the frequency scanning, which may lead to greater robustness against these effects.

3.4 Swirling flow at 0 D

For this flow configuration, the location of the axial swirler is changed to a position as close as possible to the measurement plane. A comparison of the resulting velocity, pressure and temperature maps is shown in Figure 8. The axial velocity field is heavily deformed by the swirler. The four struts of the support structure on the outer radius imprint a subdivision of the velocity field into four zones. The flow field in the area close to the axis shows the influence of the four swirler vanes. Finally, the central support causes flow separation and a recirculation zone, that is characterized by the negative axial velocities in the center. The in-plane velocities show the general clockwise rotation induced by the swirler. Additionally, the both components exhibit a strong

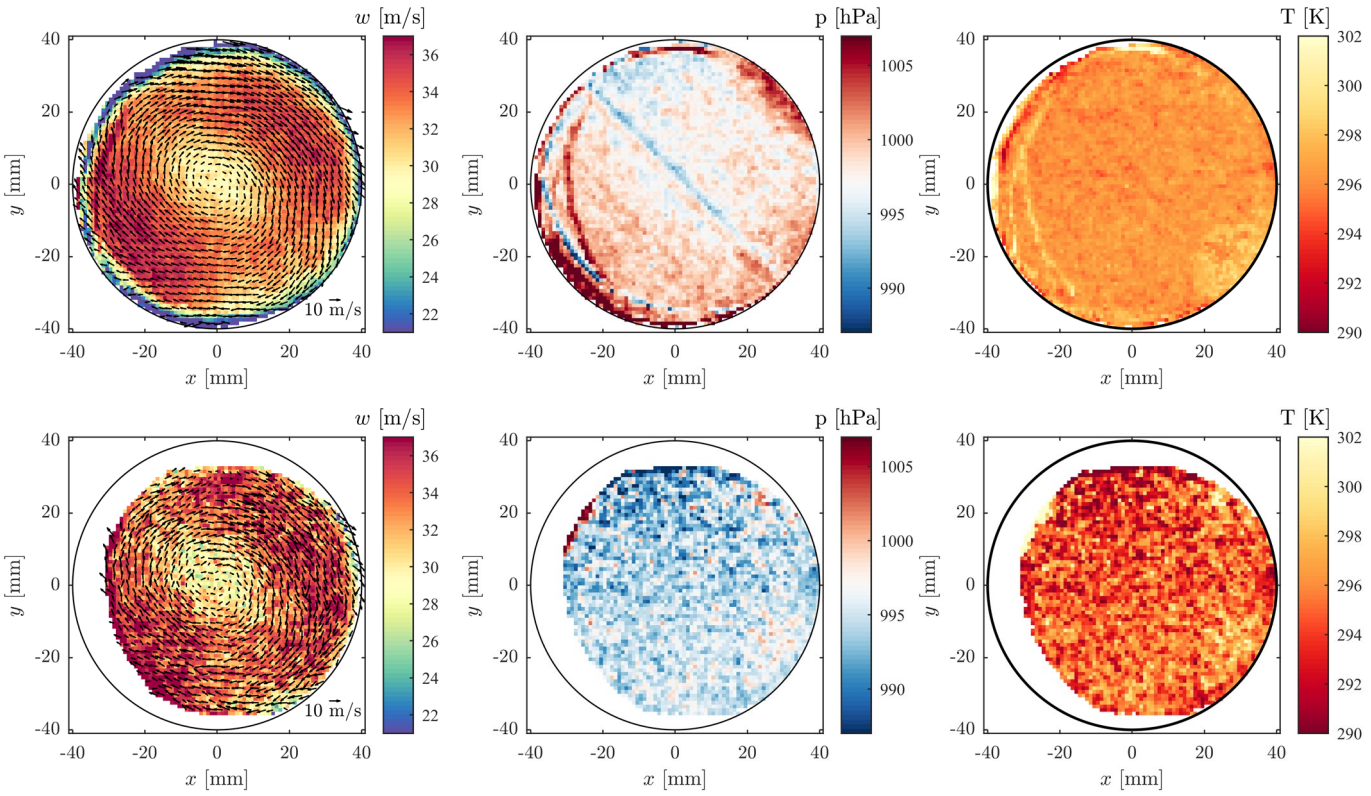

Figure 7: Comparison of velocity (left), pressure (middle) and temperature (right) maps obtained with frequency scanning (top) and single-fequency analysis (bottom) for the 0D configuration. The velocity maps show the main component w as contour variable, the in-plane components (u, w) as vector field.

impact of the swirler structure as well, resulting in a complex flow pattern. All these details are captured well with both frequency scanning and single-frequency processing methods.

The temperature is again expected to be constant over the cross section, which is well captured with both methods. Beside the artifacts that are discussed above, the pressure field obtained with the frequency scanning method exhibits a low-pressure region that clearly resembles shape of the swirler vane channels. This structure is not visible with the single-frequency processing, which indicates that the sensitivity of the method is not sufficient to resolve it.

4. Conclusion and outlook on implementation challenges

The simultaneous measurement of multiple flow properties by FRS is typically achieved by time-consuming frequency scanning. This paper expands on our recently introduced methodology (Doll et al., 2024), that uses six optimized observation directions to obtain planar pressure, temperature and 3C velocity fields from an FRS measurement based on a single excitation frequency. In a circular duct flow experiment, it is found that reference pressures and temperatures are reproduced with an accuracy of 3.4% and 1.3% respectively. In comparison with corresponding LDA measurements of axial velocities, an excellent agreement within ± 2 m/s is

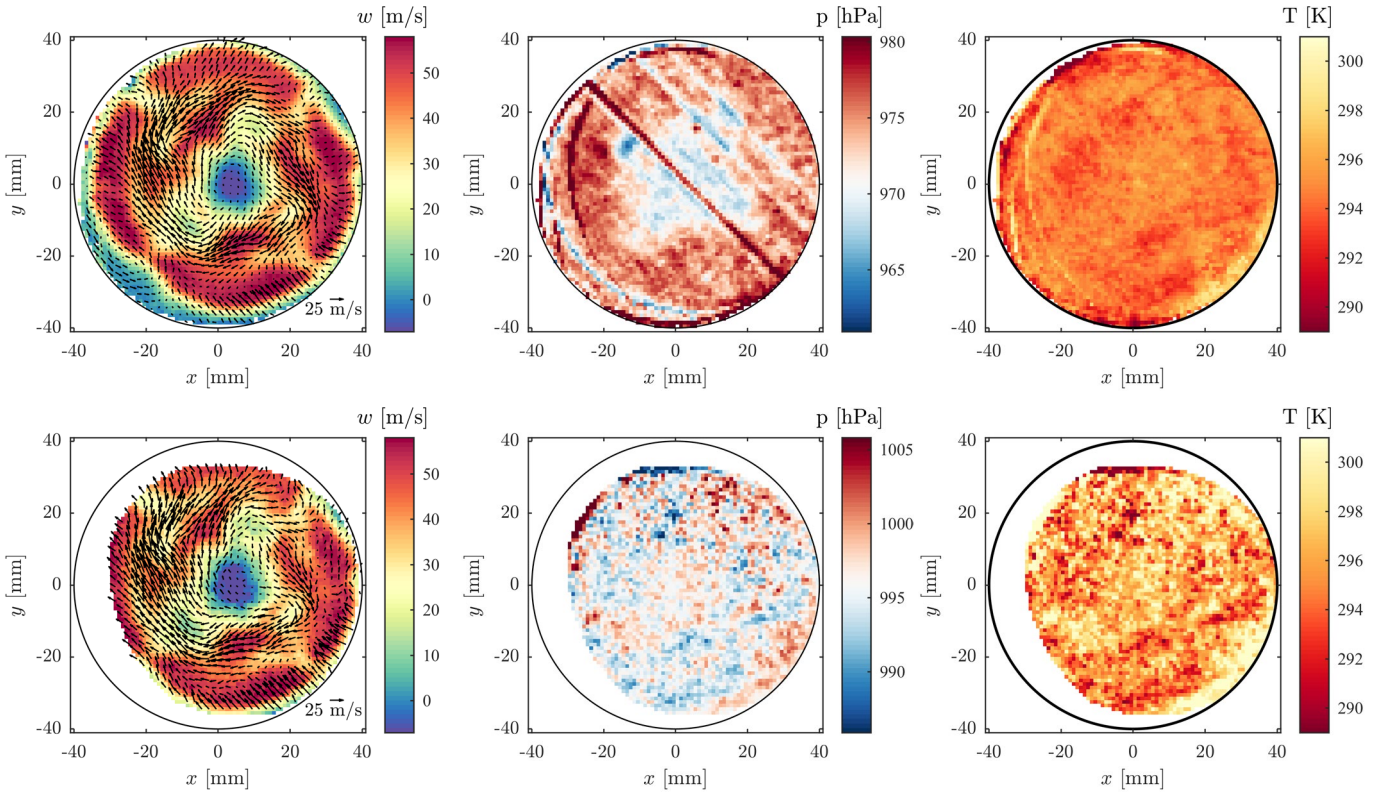

Figure 8: Comparison of velocity (left), pressure (middle) and temperature (right) maps obtained with frequency scanning (top) and single-fequency analysis (bottom) for the 0D configuration. The velocity maps show the main component w as contour variable, the in-plane components (u, w) as vector field. Please note that the pressure colormaps are on slightly different levels but have the same range.

found for all operating points. Concerning precision, a newly developed multistage evaluation procedure enables values for pressure, temperature and velocity as low as 3 hPa, 2.2 m/s and 1.7 m/s.

The secondary flow pattern induced by an axial swirler 7 diameters upstream from the measurement plane is well resolved with the single-frequency processing. Even though confined to a smaller area of the duct´s cross section and characterized by higher spatial noise, the single-frequency results appear less prone to frequency dependencies of the calibration and background constants, that lead to artifacts in the frequency scanning pressure results. When the swirler is placed at 0 diameters from the measurement plane, the single-frequency processing captures the significant deformation of the axial velocity field and the in-plane velocity components very well. However, the impact of the swirler vane flow on the static pressure field that is well visible in the frequency scanning results does not appear for the single-frequency analysis, which may point to an insufficient sensitivity for the current data quality.

In a prove of concept approach, this paper shows that the measurement of 3C velocity, pressure and temperature with a six-view, single-frequency FRS instrument is feasible. To achieve multi-

property time-resolved measurements with the proposed multiple-view imaging concept, pulsed laser radiation will have to be used. However, considering the CW laser power of 5 W, 20 s exposure time and 5 repetitions per frequency applied in this work, this would require a laser energy of 500 J per pulse to for an equivalent signal-to-noise ratio. From this number it is apparent that the goal of single-frequency multi-property FRS is clearly not achievable by just exchanging the laser system. Nevertheless, a very powerful light source will be needed, realistically of the order of 2 J per pulse. A first measure would be to reduce the light sheet height, which is 100 mm in the current study. Second, the iodine filter used herein offers significant optimization potential: (1) The transmitted Rayleigh intensity at the optimized laser frequency is below 10% for 5 of the six perspectives (Figure 1, right, bottom) and there is huge potential for increasing signals. (2) The current iodine filter cell was designed for compactness combined with high peak absorption. Therefore, a comparably high iodine vapor pressure is used, which comes with the caveat of a very high continuum absorption that could be significantly reduced with a longer filter design. Third, the number of perspective views could be raised, which would improve the evaluation quality with a more intensities per resolution element. Additionally, the image fiber bundle has a specified transmission of 40%. This technology is around for several decades and there is reason to believe that progress in optical fiber technology could lead to improvements. Finally, all system components (e.g. camera, camera lenses, bandpass filter, transfer optics, etc.) should be revisited and selected for maximum sensitivity. Taking all these measures into account, there is the very realistic chance that the combined time-resolved measurement of pressure, temperature and 3C velocity fields by FRS will become a reality.

Acknowledgements

The SINATRA project leading to this publication has received funding from the Clean Sky 2 Joint Undertaking (JU) under grant agreement No 886521. The JU receives support from the European Union's Horizon 2020 research and innovation programme and the Clean Sky 2 JU members other than the Union.

References

Boguszko, M., & Elliott, G. S. (2005). On the use of filtered Rayleigh scattering for measurements in compressible flows and thermal fields. *Experiments in Fluids*, *38*(1), 33–49. https://doi.org/10.1007/s00348-004-0881-4

Doll, U., Kapulla, R., Dues, M., Steinbock, J., Melnikov, S., Röhle, I., Migliorini, M., & Zachos, P. K. (2024). Towards time-resolved multi-property measurements by filtered Rayleigh scattering: Diagnostic approach and verification. *Experiments in Fluids*, *65*(2). https://doi.org/10.1007/s00348-023-03740-6

Doll, U., Röhle, I., Dues, M., & Kapulla, R. (2022). Time-resolved multi-parameter flow diagnostics by filtered Rayleigh scattering: System design through multi-objective optimisation. *Measurement Science and Technology*, *33*(10), 105204. https://doi.org/10.1088/1361-6501/ac7cca

Doll, U., Stockhausen, G., & Willert, C. (2014). Endoscopic filtered Rayleigh scattering for the analysis of ducted gas flows. *Experiments in Fluids*, *55*(3), 1690. https://doi.org/10.1007/s00348-014-1690-z

Doll, U., Stockhausen, G., & Willert, C. (2017). Pressure, temperature, and three-component velocity fields by filtered Rayleigh scattering velocimetry. *Optics Letters*, *42*(19), 3773–3776. https://doi.org/10.1364/OL.42.003773

Forkey, J. N., Finkelstein, N. D., Lempert, W. R., & Miles, R. B. (1996). Demonstration and characterization of filtered Rayleigh scattering for planar velocity measurements. *AIAA Journal*, *34*(3), 442–448. https://doi.org/10.2514/3.13087

Miles, R. B., Lempert, W. R., & Forkey, J. N. (2001). Laser Rayleigh scattering. *Measurement Science and Technology*, *12*(5), R33–R51. https://doi.org/10.1088/0957-0233/12/5/201

Miles, R., & Lempert, W. (1990). Two-dimensional measurement of density, velocity, and temperature in turbulent high-speed air flows by UV rayleigh scattering. *Applied Physics B Photophysics and Laser Chemistry*, *51*(1), 1–7. https://doi.org/10.1007/BF00332317